crystals

MDPI

Article

Synthesis, X-ray Crystal Structure, Hirshfeld Surface Analysis, and Molecular Docking Study of Novel Hepatitis B (HBV) Inhibitor: 8-Fluoro-5-(4-fluorobenzyl)-3-(2-methoxybenzyl)-3,5-dihydro-4H-pyrimido[5,4-b]indol-4-one

Aleksandr V. Ivashchenko [1], Oleg D. Mitkin [1,*], Dmitry V. Kravchenko [2], Irina V. Kuznetsova [2], Sergiy M. Kovalenko [1,3], Natalya D. Bunyatyan [3,4] and Thierry Langer [5]

[1] ChemRar Research and Development Institute, 7 Nobel st., Innovation Center Skolkovo territory, 143026 Moscow, Russia
[2] Chemical Diversity Research Institute, 2A Rabochaya st., Khimki, 141400 Moscow Region, Russia
[3] Federal State Autonomous Educational Institution of Higher Education I.M. Sechenov First Moscow State Medical University of the Ministry of Healthcare of the Russian Federation (Sechenovskiy University). 8 Trubeckaya st., 119991 Moscow, Russia
[4] Federal State Budgetary Institution "Scientific Centre for Expert Evaluation of Medicinal Products" of the Ministry of Health of the Russian Federation, Petrovsky boulevard 8, bld. 2, 127051 Moscow, Russia
[5] Department of Pharmaceutical Chemistry, University of Vienna, Althanstraße 14, A-1090 Vienna, Austria
* Correspondence: mod.chemdiv@gmail.com; Tel.: +7-495-995-4941 (O.D.M.)

Received: 6 June 2019; Accepted: 18 July 2019; Published: 24 July 2019

Abstract: A method for the synthesis of 8-fluoro-5-(4-fluorobenzyl)-3-(2-methoxybenzyl)-3,5-dihydro-4H-pyrimido[5,4-b]indol-4-one has been developed and the electronic and spatial structure of a new biologically active molecule has been studied both theoretically and experimentally. The title compound was crystallized from acetonitrile and the single-crystal X-ray analysis has revealed that it exists in a monoclinic $P2_1/n$ space group, with one molecule in the asymmetric part of the unit cell, a = 16.366(3) Å, b = 6.0295(14) Å, c = 21.358(4) Å, β = 105.21(2)°, V = 2033.7(7) Å^3 and Z = 4. Hirshfeld surface analysis was used to study intermolecular interactions in the crystal. Molecular docking studies have evaluated the investigated compound as a new inhibitor of hepatitis B. Testing for anti-hepatitis B virus activity has shown that this substance has in vitro nanomolar inhibitory activity against Hepatitis B virus (HBV).

Keywords: hepatitis B; HBV; pharmaceutical crystals; 3,5-dihydro-4H-pyrimido[5,4-b]indol-4-one; 1H-indole; pyrimidin-4(3H)-one; hydrogen bond; Hirshfeld surface analysis; molecular docking study

1. Introduction

Despite significant progress in the etiology of viral hepatitis studying, the incidence of this disease remains quite high. Therefore, the problem of viral hepatitis is one of the most actual ones in modern medicine. According to the World Health Organization data, 240 million people worldwide suffer from chronic infection and are carriers of HBV. About 780 thousand people die each year from diseases associated with hepatitis B [1]. Currently, drugs to suppress viral replication are available, but a complete cure is rarely achieved. Therefore, the search for new drugs for the treatment of hepatitis B is an actual and important task.

Nitrogen-containing heterocycles play a key role among the multitude of biologically active heterocycles [2–6]. Recently, a literature search exposed that a large number of molecules currently under investigation contain nitrogen heterocycles, and of these, 1H-indoles and pyrimidin-4(3H)-ones form a very substantial type of compounds. These heterocycles have the "privileged" indole framework which is commonly found in natural products and pharmaceutical drugs [7–12]. Pyrimidoindole moieties [13–15] are important structural motifs which are found in numerous pharmaceutically active compounds. They have revealed a wide range of high biological activity, such as antihypertensive and anti-inflammatory [16], anti-asthma [17,18], and act as α1-adrenergic receptor ligands or A1 adenosine receptor antagonists [19], potential tyrosine kinases (PTK) inhibitors, CFR1 and neuropeptide Y receptor ligands [20]. Despite the large spectrum of biological activity of these moieties, this range can be supplemented by introducing certain functional groups. Therefore, it is of substantial interest to develop efficient methods for the synthesis of such structures and their derivatives.

In a continuation of our efforts to obtain new HBV inhibitors for treatment and prevention of human HBV infections [21,22], we initiated the design, synthesis, and anti-hepatitis B virus activity testing of a new 8-fluoro-5-(4-fluorobenzyl)-3-(2-methoxybenzyl)-3,5-dihydro-4H-pyrimido[5,4-b] indol-4-one. Single-crystal X-ray analysis and different spectroscopic techniques assured the assigned chemical structure of the title compound. In addition, molecular docking simulations and study were also executed for the title compound.

2. Results and Discussion

In frames of the development of a platform for biologically active compound libraries, design for actual biotargets, including platform testing on the example of the invention and preparation of candidate libraries for HBV treatment designed as inhibitors of viral penetration and assembly of viral core particles, we have carried out a pilot in vitro screening of a series of new compounds. At the first stage of the cytotoxicity pilot screening, all the potential inhibitors of viral infection were studied, of which about 1000 showed cytotoxicity over 50% at 10 μM. At the second stage of the screening from 27,297 substances with a cytotoxicity not exceeding 50%, 404 molecules were selected, which showed the ability to reduce the concentration of the HBV infection development marker HBeAg at the same concentration. It has been found that a quite promising molecular scaffold for the creation of a new potent drug for the treatment of hepatitis B is 3,5-dihydro-4H-pyrimido[5,4-b]indol-4-one (Figure 1).

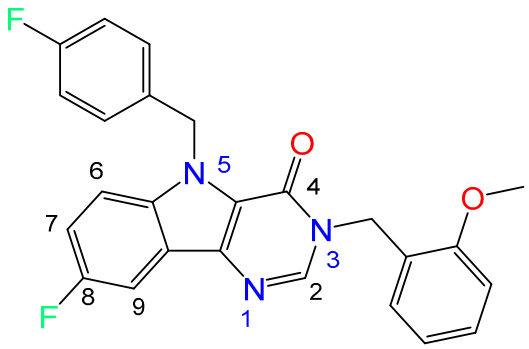

Figure 1. Chemical structure of title compound (**3**).

2.1. Synthesis

The synthesis of the title Compound (**3**) (Scheme 1) was carried out in several stages. The starting methyl 3-amino-5-fluoro-1-(4-fluorobenzyl)-1H-indole-2-carboxylate (**1**) was obtained according to the method described in Reference [23]. A further product (**1**) was converted to 8-fluoro-5-(4-fluorobenzyl)-3,5-dihydro-4H-pyrimido[5,4-b]indol-4-one (**2**) by boiling in formamide, and subsequent alkylation in DMF in the presence of sodium hydride led to the title Compound (**3**).

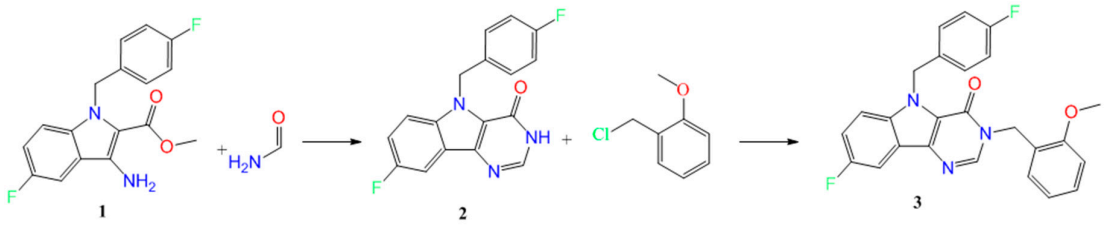

Scheme 1. Synthesis of the 8-fluoro-5-(4-fluorobenzyl)-3-(2-methoxybenzyl)-3,5-dihydro-4H-pyrimido[5,4-b]indol-4-one (**3**).

2.2. Crystal and Molecular Structure Analysis

The structure of Compound (**3**) was studied using different spectral methods (see Materials and Methods and Supporting information) and finally confirmed using XRD analysis.

The crystallographic information and refinement data are presented in Materials and Methods. Table S1 illustrates the bond angles and bond lengths (See Supporting information).

The unit cell asymmetric part of the studied crystal contained one molecule of the title Compound (**3**) (Figure 2). All atoms of the tricyclic fragment lay in the plane within 0.01 Å. The presence of vicinal substituents in the pyrimidinone cycle resulted in some nonequivalence of the Csp^2–N bonds: the C2-N1 bond (1.400(6) Å) was longer as compared to the C1-N1 bond (1.369(6) Å) and the mean value for the Csp^2–N bond (1.355 Å). The ortho-methoxy-phenyl fragment of the substituent at N1 atom was orthogonal to the bicyclic fragment (the C1-N1-C18-C19 torsion angle was 93.6 (4)°) and it was turned with respect to the N1-C18 bond (the N1-C18-C19-C20 torsion angle was -29.1(6)°). Such a position of this group resulted in the appearance of the H18B···O1 2.43 Å (the van der Waals radii sum was 2.46 Å) and H18B···O2 2.32 Å (2.46 Å) shortened intramolecular contacts, which cannot be considered as hydrogen bonds owing to the very small value of the C-H···O angles (97° and 102° respectively). The formation of the C20-H20···C1(π) intramolecular hydrogen bond (Table 3) was presumed to be stabilizing for such a position of this fragment. The methoxy group was slightly non-coplanar to the aromatic cycle (the C25-O2-C24-C23 torsion angle was 8.7(7)°) despite the essential repulsion between hydrogen atoms of the methyl group and cyclic atoms (the shortened intramolecular contacts were H23···H25A 2.32 Å (the van der Waals radii sum [24] was 2.34 Å), H25A···C23 2.78 Å (2.87 Å)). The para-fluorophenyl fragment of the substituent at N3 atom was located in the ac-conformation relatively to the C3-N3 endocyclic bond (the C3-N3-C11-C12 torsion angle was −78.3(5)°) and it was turned significantly with respect to the N3-C11 bond (the N3-C11-C12-C17 torsion angle was −50.7(5)°).

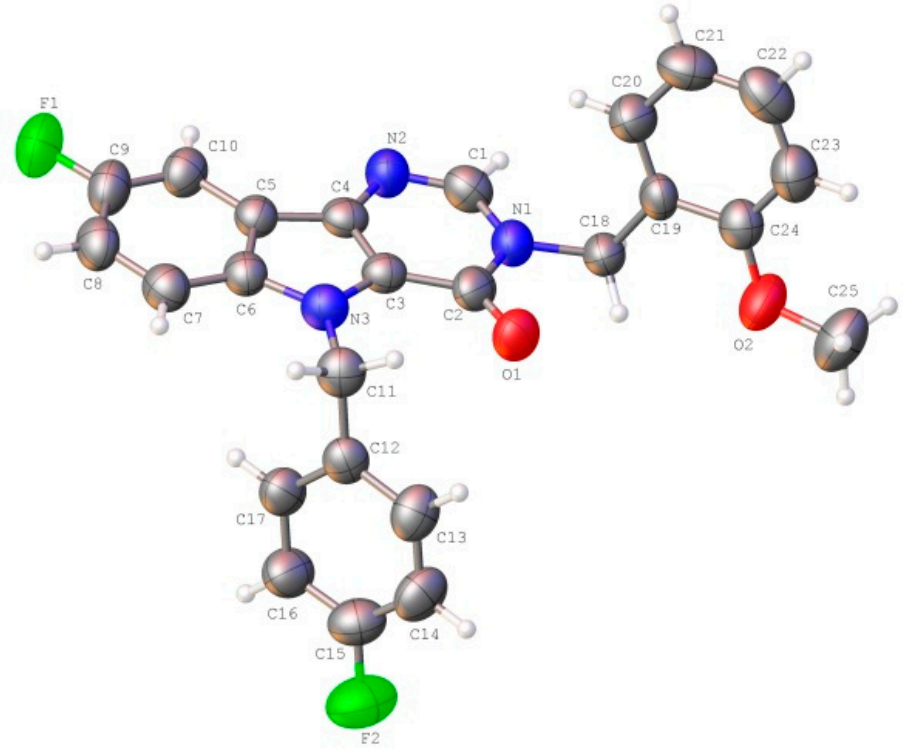

Figure 2. The molecular structure of the title Compound (**3**), showing the atom labeling. Displacement ellipsoids are drawn at the 50% probability level.

Most drugs are used in the solid-state, therefore special attention should be paid to the intermolecular interactions and features of the crystal structure.

In the crystal phase, molecules (**3**) formed centrosymmetric dimers (Figure 3) due to the C1-H1…F1 and C10-H10…N2 intermolecular hydrogen bonds (Table 1). These dimers were bound by stacking interactions (C…C 3.29 Å and shift 4.99 Å, angle between planes 0°) and weak C25-H25A…C21(π) intermolecular hydrogen bonds (Table 1) forming columns (Figure 4) along the [0 1 0] crystallographic direction. The molecules of the neighboring columns were bound by the C23-H23…C9(π) and C14-H14…O1 intermolecular hydrogen bonds (Table 1). Moreover, the H25…H14 intermolecular short contact (2.22 Å (2.32 Å)) has been revealed in the crystal.

Table 1. Hydrogen bond characteristics (Å, °) in the crystal of Compound (**3**).

D—H···A	D—H	H···A	D···A	D—H···A
C1—H1···F1^{i}	0.93	2.60	3.433(5)	149.0
C10—H10···N2^{i}	0.93	2.53	3.417(6)	159.8
C14—H14···O1^{ii}	0.93	2.56	3.346(5)	143.1
C20—H20···C1	0.93	2.79	3.381(6)	122.5
C23—H23···C9^{iii}	0.93	2.87	3.668(6)	144.3
C25-H25A…C21^{iiii}	0.93	2.74	3.572(3)	144.9

Symmetry codes: (i) –x + 1, −y + 1, −z + 1; (ii) −x, −y + 2, −z + 1; (iii) x−1/2, −y + 3/2, z−1/2; (iiii) x, 1 + y, z.

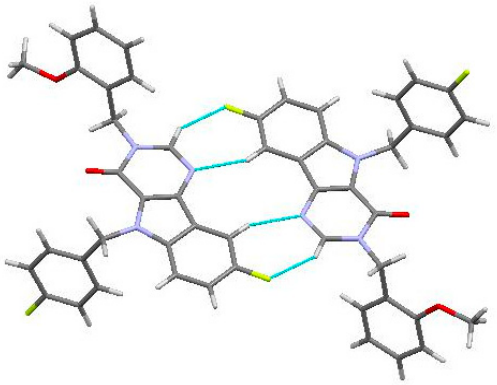

Figure 3. Centrosymmetric dimer in the crystal of titled Compound (**3**).

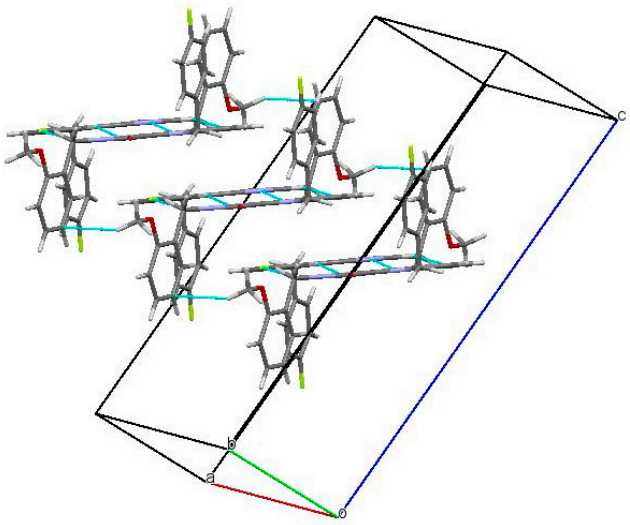

Figure 4. Columns of the dimers in the crystal phase.

2.3. Hirshfeld Surface Analysis

The peculiarities of the crystal packing were caused by the capability of the molecule to form certain types of intermolecular interactions. On the other hand, the biological activity depends on the formation of intermolecular interactions between the target molecule and the corresponding receptor. Thus the study of intermolecular interactions is a very important task.

One of the newest methods for intermolecular interactions analysis in the crystal phase is the study of Hirshfeld surfaces and 2D fingerprint plots generated using the CrystalExplorer program [25]. The Hirshfeld surfaces and their associated 2D fingerprint plots for the title Compound (**3**) were calculated taking the data of the single-crystal X-ray crystal structure as input. The Hirshfeld surface emerged from an attempt to define the space occupied by a molecule in a crystal for the purpose of partitioning the crystal electron density into molecular fragments [26]. It provided a 3D picture of the close contacts in the crystal, and these contacts can be summarized in a fingerprint plot [27]. The areas of the short contacts are shown by a red color on the Hirshfeld surfaces, while the long distances can be detected as the blue areas (Figure 5). The intermolecular interactions outward the H···H/C···H/F···H/O···H/N···H/C···C/C···N/C···F/C···O/N···F contacts, as well as the overall fingerprint region of the title molecule, are displayed in Figure 5. With this analysis, the division of contributions is possible for different interactions including H···H, N···H, C···H, and O···H, which commonly overlap in the full fingerprint plots. Figure 6 shows the d_{norm} surface of Compound (**3**), the contribution from the C…H/H…C contacts, corresponding to the C—H…π interaction, is

represented by a pair of sharp spikes (29.0%). The absence of long sharp spikes indicates the absence of strong hydrogen bonds in the crystal of the title Compound (**3**) (Figure 6).

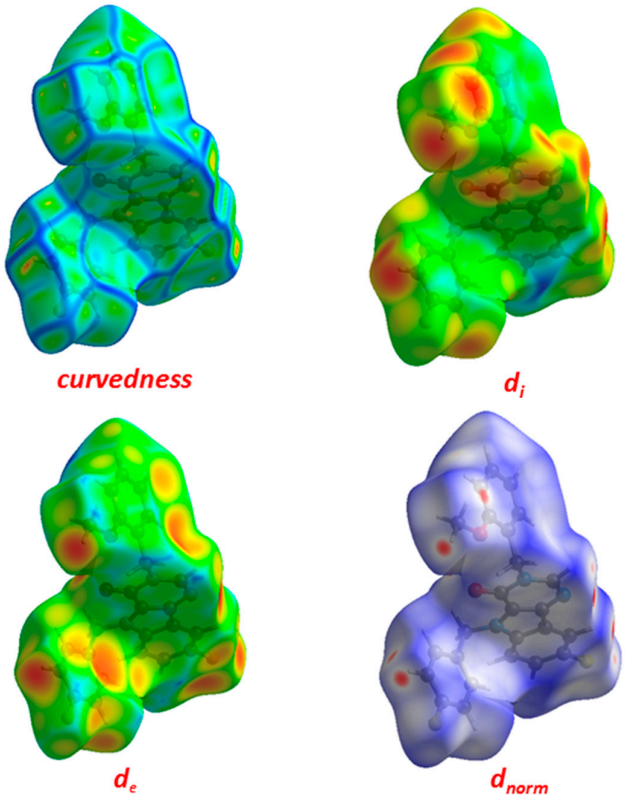

Figure 5. Hirshfeld surfaces for d_{norm}, d_i, and d_e and curvedness for Compound (**3**).

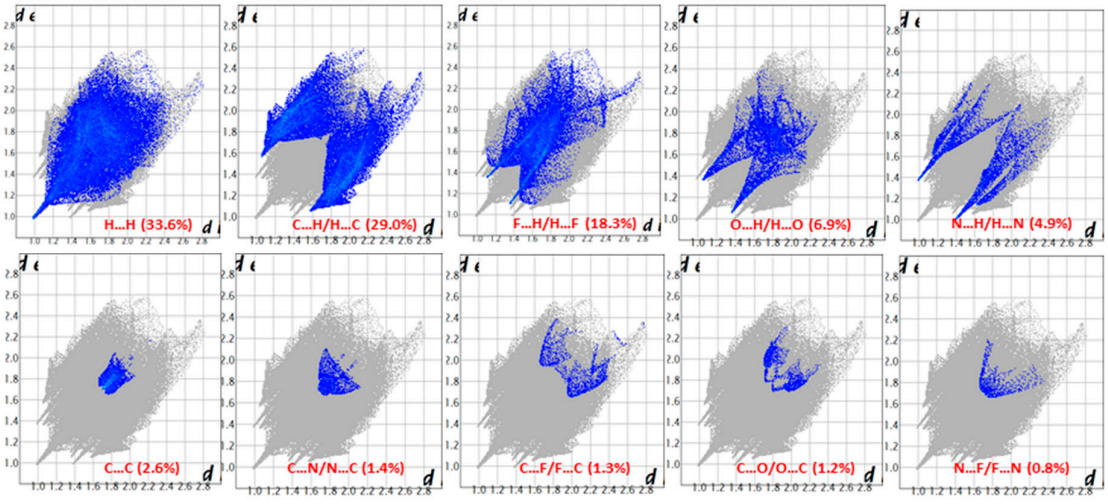

Figure 6. Two-dimension fingerprint plots showing various intermolecular contacts in Compound (*3*).

2.4. Quantum Chemistry Calculations of Geometry and Electronic Structure

Using computational methods to study properties of potentially biologically active molecules allows us to predict its behavior in the real environment. At the first stage, we have performed the optimization of the title molecule in a vacuum (using M062x DFT functional with cc-pVDZ basis set

to estimate the influence of polar environment and crystal packing effects. Essentially we are interested in torsion angles values since they are closely related with effects of embedding of the ligand into the protein molecule.

Table 2. Geometrical parameters of the title compound (bond lengths in Å, torsion angles presented in degrees, numeration of atoms according to Figure 2).

Bond / Torsion Angle	Experimental Value (X-ray Study)	Calculated Value, (Vacuum)
F1–C9	1.358(5)	1.345
F2—C15	1.366(5)	1.342
O1—C2	1.221(5)	1.227
O2—C24	1.362(5)	1.354
O2—C25	1.425(5)	1.411
N1—C1	1.369(5)	1.377
N1—C2	1.400(5)	1.404
N1—C18	1.460(4)	1.472
N2—C1	1.289(5)	1.292
N2—C4	1.375(5)	1.371
N3—C3	1.385(5)	1.377
N3—C6	1.395(5)	1.381
N3—C11	1.449(5)	1.459
C1–N1–C12–C19	93.6	58.5
N1–C18–C19–C20	−29.1	−116.1
C25–O2–C24–C23	8.7	1.7
C3–N3–C11–C12	−78.3	−94.6
N3–C11–C12–C17	−50.7	−106

As one can see, the calculated bond lengths were rather close to those obtained in the crystal phase (Table 2). However, the results for torsion angles, which correspond to rotation around single bonds, demonstrated significant differences between the X-ray and calculated values. It is obvious that such differences were connected with the packing effects.

In addition to the above mentioned geometric configuration (Conf. A), there were several conformations that are important in the description of the biological activity. They were generated by rotating around single bonds N3-C11, N1–C18 and C18–C19 (see Figure 2). Two additional conformations obtained in ab initio calculations are presented in Figure 7. The energy differences between the above-mentioned conformers were rather small—0.25 kcal/mol. Some comparisons of the ab initio results with the docking results will be presented in the next section.

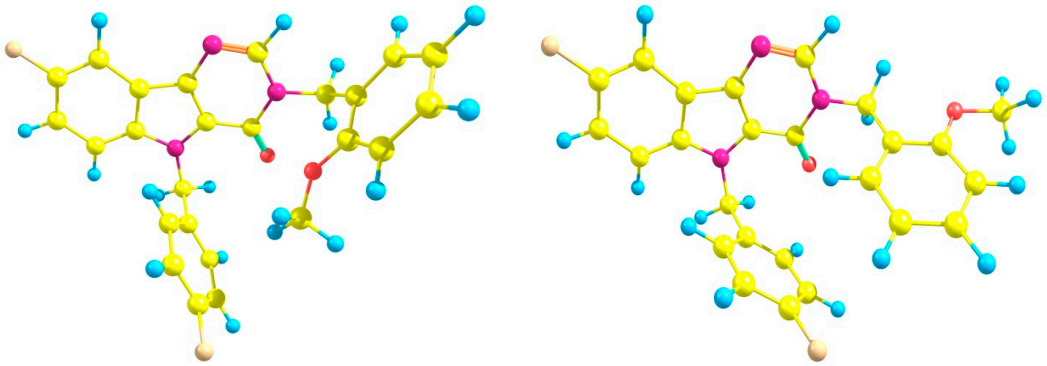

Conf. B Conf. C

Figure 7. Two additional conformations of the title system (**3**).

In the structure-activity investigation, it is useful to describe the electronic structure of the molecule. The localization of the frontier molecular orbitals (FMOs) determines the reactivity and the ability to form intermolecular complexes. Therefore we present the orbital pictures for HOMO (highest occupied molecular orbital) and LUMO (lowest unoccupied molecular orbital) in Figure 8. Corresponding orbital energies were E(HOMO) = −6.8355, E(LUMO) = −0.5129 eV. The value of E(HOMO) and a rather large value of the HOMO–LUMO gap characterize the chemical system as relatively hard with electron donating properties.

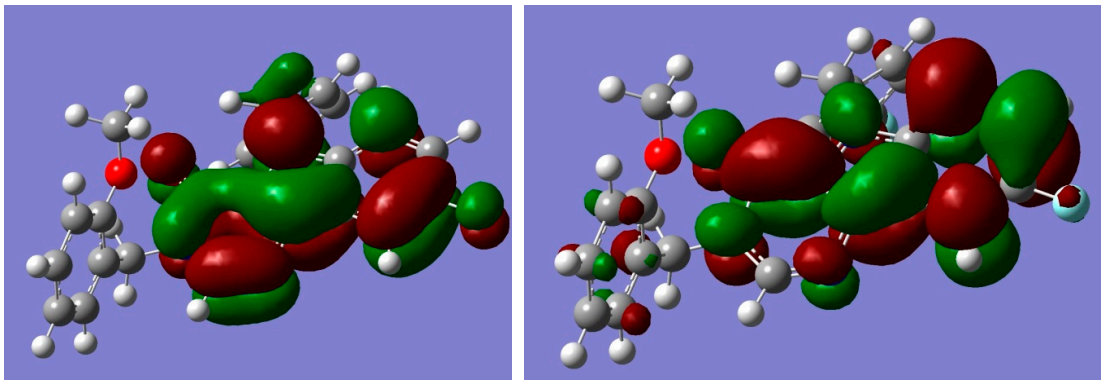

Figure 8. Graphical representation of frontier molecular orbitals (FMOs) of compound (**3**); left picture corresponds to highest occupied molecular orbital (HOMO), right— lowest unoccupied molecular orbital (LUMO).

According to our calculations, the HOMO and LUMO π-orbitals were localized at pyrimido[5,4-b]indol fragment of the molecule.

Good reproducibility of experimental data by quantum chemistry calculations indicates the possibility of using molecular modeling methods to estimate the potential interaction of the target molecule with receptors before conducting experimental tests on the biological activity.

2.5. Molecular Docking Simulations

The title molecule (**3**) has been tested as a system which interacts with the capsid of HBV (Hepatitis-B virus). Nowadays, the main approach to anti-HBV is connected with the development of new agents which are highly potent inhibitors of HBV replications [28]. Among the prospective agents which strongly interact with corresponding key proteins are derivatives of heteroaryldihydropyrimidine (HAP) [28–30]. Investigations of HAP (among them the most important chemical compounds—BAY41-4109, BAY39-5493, NVR-010-001-E2 [31–33]) demonstrated effective interactions with the corresponding HBV capsid and newly synthesized core protein. After interaction, the core protein could not assembly properly.

The compound we investigated in the present article can be treated as a structural analog of HAP. It is why we performed in silico modeling of interaction with corresponding core proteins. Fortunately for the different key ligand-proteins complexes (5T2P, 5WRE, 5GMZ, 5E0I), the X-ray crystallographic structures are known. In the present work, the 3D crystal structure of core proteins HBV bound to reference core molecules was retrieved from Reference [34].

The pharmacophore model and docking procedure have been performed by using Ligandscout 4.3. The software was provided by Reference [35]. All the above-mentioned structures of proteins contained six chains (designated as A, B, C, D, E, and F). At the first stage of our calculations, the residual mean square deviation (RMSD) between the docking-generated poses for the reference molecule and those obtained from the crystal structure X-ray investigations were calculated. As it was obtained the minimal values of RMSD, calculated for all the above-mentioned proteins, corresponded to the D-chain, where RMSD < 1 Å. The active site was found by using LigandScout option for pharmacophore generation. After that, the title molecule was docked at the corresponding site. The obtained data for score functions were collected in Table 3. In The table, the data

corresponding to the reference core molecules is also presented. It can be seen that the title molecule interacted effectively with the protein. At the same time, the interaction parameters were comparable and even better than the corresponding values obtained for the reference molecules.

Table 3. Parameters of the binding affinity of the title molecule (**3**) for a site on the D chains.

PDB	Molecule	Affinity (kcal/mol)	Binding Affinity Score
5E0I	NVR10-001E2	−21.6	−28.6
	molecule (**3**)	−17.9	−33.5
5GMZ	4-methyl heteroaryldihydropyrimidine	−16.18	−25.95
	molecule (**3**)	−16.30	−31.02
5WRE	HAP-R01	−21.46	−38.45
	molecule (**3**)	−15.16	−23.39
5T2P	SBA-R01	−15.81	−26.70
	molecule (**3**)	−17.14	−44.42

As an example, the position receptor-ligands complex (5E0I) can be seen in Figure 9. The 2D representation of the structural formula of the ligands demonstrated its correspondence to the generated pharmacophore. Here, the hydrogen bond acceptor is designated by the red dotted line, while the hydrophobic interaction is designated by the yellow line. For the detailed descriptions of the pharmacophore designation and generation, see the LigandScout manual [35].

The geometric structure of the ligand in this complex for case A was qualitatively close to conformation C while for case B—to the conformation B (see Figure 7). Comparison of most important torsion angles is presented in Table 4. Here, the numeration of atoms is in accordance with Figure 2.

Table 4. Torsion angles of ligands obtained by ab initio and docking (5E0I protein) calculations.

Torsion Angle	Docking Case A	*ab Initio* Conf. C	Docking Case B	*ab Initio* Conf. B
N3–C11–C12–C17	−3.6	53.6	30.9	19
N1–C18–C19–C24	−176.1	−170	63.2	60

As one can see, the torsion angle N3–C11–C12–C17 underwent significant changes when the ligand was incorporated into the protein.

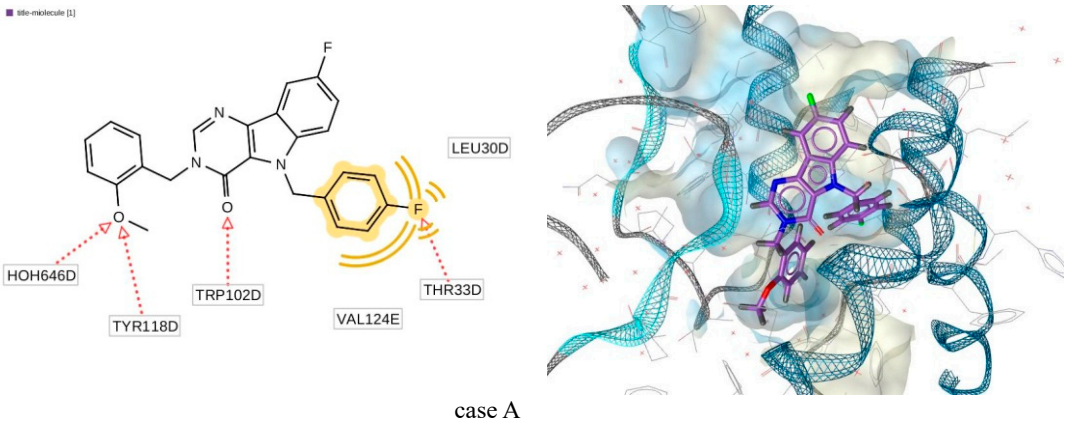

case A

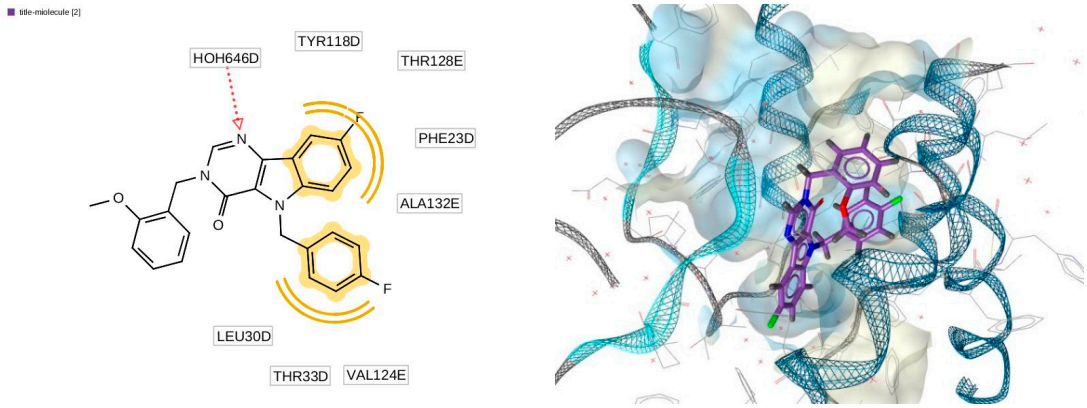

Figure 9. Generated docking pose for complex "title molecule (**3**)—5E0I".

The simulation study of the 3D binding of the title molecule with corresponding proteins demonstrated effective interaction and hence can be treated as a potent inhibitor of HBV replications.

2.6. Anti-Hepatitis B Virus (HBV) Activity

The final stage of our investigation was the experimental study of the biological activity of molecule (**3**). The human hepatoma cell line HepAD38 was chosen as the source of infectious viral particles to infect the HepG2 / NTCP cell line, carrying the stable integrated HBV virus gene under the control of a tetracycline-regulated promoter, and secreting viral particles into the culture medium in the absence of tetracycline. HBV preparation was obtained using the HepAD38 line according to the following protocol: HepAD38 cells were passaged in a DMEM medium containing 10% fetal calf serum, penicillin/streptomycin and essential amino acids. The culture medium was taken once every 2 days, clarified by centrifugation (200 g, 15 min) and stored at 4 °C for no longer than 7 days. Next, dry PEG 8000 was added to the culture media to a final concentration of 7.5% and incubated at 4 °C on a rotary platform overnight. The viral precipitate was separated by centrifugation (2000 g, 30 min) and the precipitate was suspended in 1/100 of the initial volume in OPTI-MEM medium. Thus obtained viral preparation was aliquoted and stored at −80 °C.

Infection was carried out as follows: The HepG2-NTCP cell suspension was distributed to 96-well plates at 2000 cells per well. After the cells were attached (on the same or the next day), the initial solution was removed by aspiration, and 50 μL of a solution of test compounds dissolved in OPTI-MEM medium (with a final DMSO concentration of 2%) was added to each well or OPTI-MEM with 2% DMSO (in the wells of the positive and negative controls of the infection) and 50 μL of the HBV preparation diluted in OPTI-MEM with 2% DMSO (except negative infection control). After incubation for 24 h in a humidified atmosphere containing 5% CO_2, the HBV medium was removed by aspiration, and 200 μL of DMEM culture medium containing the corresponding test compounds in 10 mkM concentration was added to the cultures. The cells were additionally incubated for 6 days at 37 °C in a humidified atmosphere containing 5% carbon dioxide. Next, cell supernatants (50 μL) were analyzed for viral antigen content using a commercial HBeAg ELISA 4.0 kit (Creative Diagnostics, catalog number DEIA003) according to the kit manufacturer's protocol and the optical density of each analyzed well was measured at a wavelength of 450 nm using a plate densitometer.

The title molecule (**3**) in an experimental in vitro model of hepatitis B virus infection with the usage of human hepatoma line HepG2, was stably transfected with the NTCP gene to impart the ability to be infected with HBV and maintain a full virus replication cycle demonstrated 83 % inhibition (for 10 mkM concentration).

3. Materials and Methods

3.1. Chemistry

3.1.1. General Information

All chemicals were obtained from Sigma-Aldrich or Merck. Detailed procedure of starting methyl 3-amino-5-fluoro-1-(4-fluorobenzyl)-1H-indole-2-carboxylate (**1**) synthesis has been reported [11]. NMR spectra were registered on a Bruker DPX 300 spectrometer (Bruker BioSpin AG, Industriestrasse 26, 8117 Fällanden, Switzerland) at room temperature (298 K) on a using DMSO-d6 as a solvent and processed using Bruker XWinNMR software (International Equipment trading Ltd., Mestrenova Version 9.0 Spain, Vernon Hills, Illinois 60061, USA). Liquid chromatography mass spectrometry was developed by means of chromatography with PHENOMENEX GEMINI NX C18 110Å 4.61 × 150 mm column (0.05% TFA, gradient ACN/ H_2O), UV-detector SHIMADZU SPD-10AD VP (registered absorption at 254 nm), ELSD (evaporative light scattering detector) SEDEX-75 (S.E.D.E.R.E., PARC VOLTA-BP 27 9, Rue Parmentier 94141 Alfortville Cedex FRANCE) and API-150EX mass-spectrometer (MDS Sciex, Toronto, Canada). Elution started with 0.1 M solution of TFA in water and ended with 0.1 M solution of TFA in acetonitrile used a linear gradient at a flow rate of 0.15 mL/min and an analysis cycle time of 25 min. The FT-IR spectrum was registered in a KBr pellet with a Shimadzu IR Prestige-21 Fourier Transform Infrared (FTIR) Spectrophotometer (Shimadzu Corporation, Kyoto, Japan). The UV/Vis spectrum was registered in acetonitrile with an Agilent 8453 UV-visible Spectrophotometer. The melting point was registered with a Buchi M-560 (Buchi AG, Meierseggstrasse 40, 9230 Flawil, Swiss). Elemental analysis was performed on EuroEA-3000 CHNS-O Analyzer (Euro Vector, Via Tortona 5-20144, Milan, Italy).

3.1.2. Synthesis and Crystallization of Compound (**3**)

To a solution of compound (**2**) (1.0 mmol, 311 mg) in DMF (5 mL), 1.1 mmol of NaH was added. After 0.5h, 1-(chloromethyl)-2-methoxybenzene (1.1 mmol, 172 mg) was added dropwise to the mixture and stirred at 50 °C for 1 h. The mixture was heated for 1 h at 50 °C and then cooled down to room temperature. The solution was poured into water. The formed precipitate was collected by filtration, recrystallized from acetonitrile, filtered off, washed with acetonitrile and dried to give pure product (**3**). Yield 336 mg (78%), white crystallic powder, m.p. 154.1–154.6 °C; UV (MeOH) λmax (nm) 223, 270, 288, 298, 325, 335, 350 (Figure S1); IR (KBr): ν (cm^{-1}) 3052, 2943 2839 (C–H), 1669 (C=O), 1588, 1565, 1504, 1461, 1371, 1305, 1243, 1214, 1022, 859, 795, 754 (Figure S2); ^{1}H NMR (300 MHz, DMSO-d6): δ 8.42 (s, 1H, H-2), 7.77 (dt, J = 8.6, 3.0 Hz, 2H), 7.39 (td, J = 9.2, 2.6 Hz, 1H), 7.34–7.20 (m, 3H), 7.12–7.00 (m, 4H), 6.90 (td, J = 7.5, 1.1 Hz, 1H), 5.91 (s, 2H, 5-CH_2), 5.24 (s, 2H, 3-CH_2), 3.84 (s, 3H, OCH_3); ^{13}C NMR (75 MHz, DMSO-d6): δ 44.85 (3-CH_2), 46.64 (5-CH_2), 55.50 (OCH_3), 105.19 (d, J = 23.7 Hz, C-9), 110.95, 113.15 (d, J = 9.3 Hz), 115.37 (d, J = 21.4 Hz), 116.32 (d, J = 26.6 Hz), 120.34, 121.00 (d, J = 9.9 Hz), 122.12, 124.26, 128.84, 129.08, 129.19, 134.15 (d, J = 3.1 Hz), 135.91, 137.53 (d, J = 5.2 Hz), 145.37, 154.56, 156.98, 157.53 (d, J = 236.6 Hz, 8-CF), 161.42 (d, J = 243.5 Hz, 4′-CF); ^{19}F NMR (377 MHz, DMSO-d6): δ -121.77 (d, J = 4.3 Hz), −115.14 (Figure S3); LC/MS m/z (%): 432.5 $[MH]^+$ (99); found, %: C 69.93; H 4.40; N 9.77. $C_{25}H_{19}F_2N_3O_2$. Calculated, %: 69.60; H 4.44; N 9.74.

Further crystallization by slow evaporation of a solution in acetonitrile was carried out to provide single stick-like colorless crystals suitable for X-ray diffraction analysis (Figure 10).

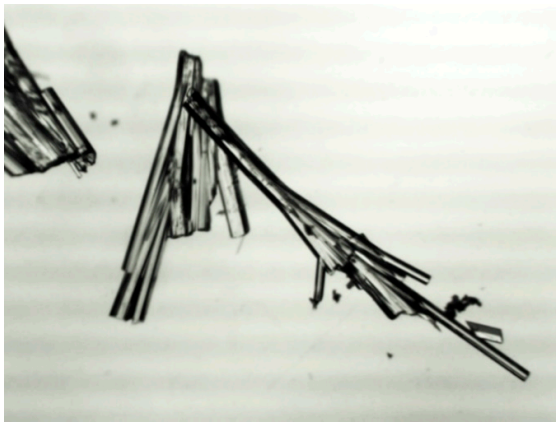

Figure 10. Crystals of the title Compound (**3**).

3.2. X-ray Diffraction Study

The crystals of (**3**) ($C_{25}H_{19}F_2N_3O_2$) were monoclinic. At 293 K a = 16.366(3) Å, b = 6.0295(14) Å, c = 21.358(4) Å, β = 105.21(2)°, V = 105.21(2) Å^3, M_r = 431.43, Z = 4, space group $P2_1/n$, d_{calc} = 1.409 g/cm^3, μ (Mo$K\alpha$) = 0.103 mm^{-1}, F(000) = 896. Intensities of 14,544 reflections (3571 independent, R_{int} = 0.1315) were measured on the «Xcalibur-3» diffractometer (graphite monochromated Mo$K\alpha$ radiation, CCD detector, ω-scaning, 2θmax = 50°).

The structure was solved by direct methods using the SHELXTL package [36]. The position of the hydrogen atoms was located from electron density difference maps and refined by the "riding" model with U_{iso} = nU_{eq} of the carrier atoms (n = 1.5 for methyl groups and n = 1.2 for other hydrogen atoms). Full-matrix least-squares refinement of the structures against F^2 in anisotropic approximation for non-hydrogen atoms using 3571 reflections was converged to: wR_2 = 0.184 (R_1 = 0.068 for 1558 reflections with $F > 4\sigma(F)$, S = 0.913).The final atomic coordinates and crystallographic data for molecule (**3**) have been deposited to with the Cambridge Crystallographic Data Centre, 12 Union Road, CB2 1EZ, UK (fax: +44-1223-336033; e-mail: deposit@ccdc.cam.ac.uk) and are available on request quoting the deposition number CCDC 1915665).

3.3. Theoretical Calculations

Crystal Explorer 17.5 was utilized to generate fingerprint plots and Hirshfeld surface map of the title compound (**3**) [25]. All quantum chemical calculations were carried out using Gaussian 09 [37].

3.4. Docking Studies

The pharmacophore model generation and docking were performed using Ligandscout 4.3 program [35].

4. Conclusions

The new biologically active compound (8-fluoro-5-(4-fluorobenzyl)-3-(2-methoxybenzyl)-3,5-dihydro-4H-pyrimido[5,4-b]indol-4-one) has been studied using both theoretical and experimental methods. The title compound was characterized by spectral methods and its molecular and crystal structure has been confirmed by X-ray diffraction study. Being very important to provide the interaction with receptors intermolecular interactions were studied thoroughly. Some approaches to quantum chemical modeling of possible interaction of the title molecule with receptors have been used. At the first stage, it was shown the reproducibility of experimental molecular geometry by the quantum chemical calculations. At the next stage, the interactions between the potential drug and receptors were modeled. Finally, the experimental study of biological activity has shown that a very potent drug for hepatitis B has been developed.

Supplementary Materials: The following are available online at www.mdpi.com/xxx/s1, Figure S1: UV/Vis spectrum of the title compound (3) (MeOH, M 0.0116 mmol/l, optical cell 1.0 cm), Figure S2: IR spectrum of the title compound (3) (KBr pellet), Figure S3: 19F NMR (376.72 MHz, DMSO-d6) spectrum of the title compound (3), Figure S4: 13C NMR (75.48 MHz, DMSO-d6) spectrum of the title compound (3), Figure S5: 1H NMR (300.16 MHz, DMSO-d6) spectrum of the title compound (3), Figure S6: LC/MS Data for Structural Determination of of the title compound (3), Table S1: Geometric parameters (Å, ◦) of the title Compound (3). .

Author Contributions: A.V.I. proposed the work and prepared the manuscript for publication, S.M.K. and D.V.K. synthesized and characterized the title molecule, T.L, I.V.K. and N.D.B. conducted the computational calculations, O.D.M performed the screening of anti-HBV activity. All authors discussed the contents of the manuscript.

Funding: The work was supported by the Ministry of Science and Higher Education of the Russian Federation in frames of agreement on reimbursement of costs associated with the development of a platform for biologically active compound libraries and the design of actual biotargets, including platform testing on the example of invention and preparation of candidate libraries for HBV treatment designed as inhibitors of viral penetration and assembly of viral core particles (RFMEFI57917X0154).

Acknowledgments: We thank A.N. Nesmeyanov Institute of Organoelement Compounds of Russian Academy of Sciences (INEOS RAS) for the support of the Crystallography Laboratory. The authors are grateful to Konovalova I.S. (SSI "Institute for Single-crystals", Kharkiv) for assistance with the XRD analysis.

Conflicts of Interest: The authors declare no conflict of interest.

References

1. World Health Organization (WHO). *Hepatitis B Fact Sheet N204*; WHO: Geneva, Switzerland, 2017.
2. Elguero, J.; Goya, P.; Jagerovic, N.; Silva, A.M.S. Pyrazoles as Drugs: Facts and Fantasies in Targets in Heterocyclic Systems**.** *Ital. Soc. Chem.* **2002**, *6*, 52**.**
3. Dewick, P.M. *Medicinal Natural Products: A Biosynthetic Approach*; 2nd ed; Wiley: New York, NY, USA, 2002.
4. Deiters, A.; Martin, S.F. Synthesis of Oxygen- and Nitrogen-Containing Heterocycles by Ring-Closing Metathesis. *Chem. Rev.* **2004**, *104*, 2199.
5. Agarwal, S.; Cämmerer, S.; Filali, S.; Fröhner, W.; Knöll, J.; Krahl, M.P.; Reddy, K.R.; Knölker, H.-J. Novel Routes to Pyrroles, Indoles and Carbazoles - Applications in Natural Product Synthesis**.** *Curr. Org. Chem*. **2005**, *9*, 1601.
6. Gataullin, R.R. Synthesis of compounds containing a cycloalka[b]indole fragment. *Russ. J. Org. Chem*. **2009**, *45*, 321.
7. Bolton, D.; Forbes, I.T.; Hayward, C.J.; Piper, D.C.; Thomas, D.R.; Thompson, M.; Upton, N. Synthesis and potential anxiolytic activity of 4-amino-pyrido [2, 3-b] indoles. *Bioorg. Med. Chem. Lett.* **1993**, *3*, 1941.
8. Love, B.E. Synthesis of carbolines possessing antitumor activity. *Top. Heterocycl. Chem*. **2006**, *2*, 93.
9. Somei, U.; Basha, A. Indole Alkaloids; Hawood Academic Publishers: Amsterdam, Netherlands, 1997.
10. Humphrey, G.R.; Kuethe, J.T. Practical methodologies for the synthesis of indoles. *Chem. Rev*. **2006**, *106*, 2875.
11. Sundberg, R.J. *Indoles*; 1st ed.; Academic Press: London, UK, 1996.
12. Sundberg, R.J. *Comprehensive Heterocyclic Chemistry II*, 2nd ed; Katritzky, A.R., Ress, C.W., Scriven, E.F.V., Bird, C.W., Eds.; Pergamon Press: Oxford, UK, 1996; Volume 2, p. 119.
13. Okamoto, A.; Tanaka, K.; Saito, I. Rational design of a DNA wire possessing an extremely high hole transport ability. *J. Am. Chem. Soc.* **2003**, *125*, 5066.
14. Okamoto, A.; Tanaka, K.; Saito, I.J. DNA logic gates. *Am. Chem. Soc*. **2004**, *126*, 9458.
15. Showalter, D.H.H.; Bridges, J.A.; Zhou, H.; Sercel, D.A.; McMichael, A.; Fry, D.W.J. Tyrosine Kinase Inhibitors. 16. 6,5,6-Tricyclic Benzothieno[3,2-d]pyrimidines and Pyrimido[5,4-b]- and -[4,5-b]indoles as Potent Inhibitors of the Epidermal Growth Factor Receptor Tyrosine Kinase. *Med. Chem*. **1999**, *42*, 5464.
16. Bundy, G.L.; Banitt, L.S.; Dobrowoski, P.L.; Palmer, J.R.; Schwartz, T.M.; Zimmermann, D.C.; Lipton, M.F.; Mauragis, M.A.; Veley, M.F.; Appell, R.B.; et al. Synthesis of 2, 4-Di-1-pyrrolidinyl-9H-pyrimido [4, 5-b] indoles, including antiasthma clinical candidate PNU-142731A. *Org. Process Res. Dev*. **2001**, *5*, 144.
17. Barnes, P.J.; Chung, K. F.; Page, C.P. Inflammatory mediators of asthma: An update. *Pharmacol. Rev*. **1998**, *50*, 515.

18. Howarth, P.H. The airway inflammatory response in allergic asthma and its relationship to clinical disease. *Allergy* **1995**, *50*, 13.
19. Muller, C.E.; Hide, I.; Daly, J.; Rothenhausler, K.; Eger, K. 7-Deaza-2-phenyladenines: structure-activity relationships of potent A1 selective adenosine receptor antagonists. *J. Med. Chem*. **1990**, *33*, 2822.
20. Darrow, J.W.; Maynard, G.D.; Horvath, R.F. Substituted 9h-pyridino[2,3-b]indole and 9h-pyrimidino[4,5-b]indole derivatives: Selective neuropeptide y receptor ligands. International Patent Application Publication No. WO 9951598, 1999/10/14.
21. Ivachtchenko, A.V.; Ivachtchenko, A.A.; Savchuk, N. Ph.; Rogovoj, B.; Bychko, V.V. Hepatitis B virus (HBV) inhibitor. International Patent Application Publication No. WO 2019017814, 2019/01/24.
22. Ivachtchenko, A.V.; Ivachtchenko, A.A.; Savchuk, N. Ph.; Rogovoj, B.; Bychko, V.V.; Khvat, A. Hepatitis B virus (HBV) penetration inhibitor and pharmaceutical composition for Hepatitis treatment. International Patent Application Publication No. RU 2662161, 2018/07/24.
23. Barker, A.J.; Kettle, J.G.; Faull, A.W. Preparation of substituted indoles for treatment of a disease or condition mediated by monocyte chemoattractant protein-1 (MCP-1). International Patent Application Publication No. WO 9907351 A2, 1999/02/18.
24. Zefirov, Y.V.; Zorky, P.M. New applications of van der Waals radii in chemistry. *Russ. Chem. Rev.* **1995**, *64*, 415–428.
25. Turner, M.J.; McKinnon, J.J.; Wolff, S.K.; Grimwood, D.J.; Spackman, P.R.; Jayatilaka, D.; Spackman, M.A. *Crystal Explorer 17*. The University of Western Australia: Perth, Australia, 2017.
26. Spackman, M.A.; Byrom, P.G. A novel definition of a molecule in a crystal. *Chem. Phys. Lett.* **1997**, *267*, 215–220.
27. Spackman, M.A.; Jayatilaka, D. Hirshfeld surface analysis. *Cryst. Eng. Comm.* **2009**, *11*, 19–32.
28. Endres, D.; Miyahara, M.; Moisant, P.; Zlotnick, A. A reaction landscape identifies the intermediates critical for self-assembly of virus capsids and other polyhedral structures. *Protein Sci.* **2005**, *14*, 1518–1525.
29. Stray, S.J.; Zlotnick, A. BAY 41-4109 has multiple effects on Hepatitis B virus capsid assembly. *J. Mol. Recognit.* **2006**, *19*, 542–548.
30. Choi, I.G.; Yu, YG. Interaction and assembly of HBV structural proteins: Novel target sites of anti-HBV agents. *Infect. Disord. Drug Targets* **2007**, *7*, 251–256.
31. Firdayani, A.; Arsianti, C.**;** Yanuar, A. Molecular Docking and Dynamic Simulation Benzoylated Emodin into HBV Core Protein. *J. Young Pharm.* **2018**, *10*, S20–S24.
32. Wu, G.; Liu, B.; Zhang, Y.; Li, J.; Arzumanyan, A.; Clayton, M.M.; Schinazi, R.F.; Wang, Z.; Goldmann, S.; Ren, Q.; et al. Preclinical characterization of GLS4, an inhibitor of hepatitis B virus core particle assembly. *Antimicrob. Agents Chemother*. **2013**, *57*, 5344–5354.
33. Wang, X.Y.; Wei, Z.M.; Wu, G.Y.; Wang, J.H.; Zhang, Y.J.; Li, J.; Zhang, H.H.; Xie, X.W.; Wang, X.; Wang, Z.H.; et al. In vitro inhibition of HBV replication by a novel compound, GLS4, and its efficacy against adefovir-dipivoxil-resistant HBV mutations. *Antivir Ther.* **2012**, *17*, 793–803.
34. Berman H.M.; Westbrook J.; Feng Z.; Gilliland G.; Bhat T.N.; Weissig H.; Shindyalov I.N.; Bourne P.E. The Protein Data Bank Nucleic Acids Research. **2000**, *28*, 235–242. Available online: http://www.rcsb.org/ (accessed on 24 July 2019).
35. Wolber, G.; Langer, T.; LigandScout: 3-D Pharmacophores Derived from Protein-Bound Ligands and Their Use as Virtual Screening Filters *J. Chem. Inf. Model*, **2005**, *45*, 160–169. Available online: http://www.inteligand.com/ligandscout/ (accessed on 24 July 2019).
36. Sheldrick, G.M. SHELXT - Integrated space-group and crystal-structure determination. *Acta. Cryst.* **2015**, *A71*, 3–8.
37. Frisch, M.J.; Trucks, G.W.; Schlegel, H.B.; Scuseria, G.E.; Robb, M.A.; Cheeseman, J.R.; Scalmani, G.; Barone, V.; Mennucci, B.; Petersson, G.A.; et al. Gaussian-09; Revision A.02; Gaussian, Inc.: Wallingford, CT, USA, 2009.